# The structure and properties of small Pd clusters

**José Rogan**[1]**, Griselda García**[2]**, Max Ramírez**[1]**, Víctor Muñoz**[1]**,
**Juan Alejandro Valdivia**[1]**, Xavier Andrade**[1]**, Ricardo Ramírez**[2] **and
**Miguel Kiwi**[1,2]

[1] Departamento de Física, Facultad de Ciencias, Universidad de Chile, Casilla 653,
Santiago 1, Chile
[2] Facultad de Física, Universidad Católica de Chile, Casilla 306, Santiago, 782-0436, Chile

**Abstract**
The zero-temperature minimal energy structure of small free-standing Pd clusters
($14 \leqslant N \leqslant 21$, where $N$ is the number of atoms in the cluster), their characteristics and their
magnetic configurations are investigated. Results obtained using five different
phenomenological many-body potentials (implemented in combination with a genetic algorithm
search) are refined by means of various density functional theory (DFT) techniques. The
agreement and differences between the results obtained with our procedure, using these five
potentials, are displayed in detail. While phenomenological potentials yield values that
approach the minimal energies of larger clusters, as compared with DFT results, they fail to
predict the right symmetry group for some of the clusters with $N > 14$. We find that the
minimal energy configurations are not necessarily associated with high symmetry of the atomic
arrangement. Actually, several cases of previously overlooked low symmetry structures turn out
to have lower energies than more symmetric ones.

(Some figures in this article are in colour only in the electronic version)

## 1. Introduction

For some time, nanoclusters have been the focus of attention
for physicists, chemists and applied scientists, due to their
interest to basic science and because of the variety of potential
and actual technological uses [1]. This interest is related to the
insight clusters and nanoparticles provide into the physical and
chemical properties as a function of size, since they constitute a
natural bridge between atoms and molecules on the one hand,
and the bulk limit on the other. For example, it is of interest
to determine the critical size and structure for which a cluster
exhibits quantization of the energy levels, which in turn is
closely related to the metal (or semiconductor) to insulator
transition.

On the application side we can mention, for example,
that Fe clusters promote the nitrogen plus hydrogen conversion
into ammonia, and that platinum clusters catalyze the process
used to increase the octane grade of gasoline. Gold,
silver and copper clusters are optically active in the visible
region, thus allowing the fabrication of optical devices.
Palladium, our focus of interest, is used to create catalytic
lattices [2] and, because of its nearly full d band, has unusual

magnetic properties [3]. This effect becomes more marked
in nanoclusters and is highly dependent on the particular low
energy structure, as will be seen below.

The first and crucial step in the description and
understanding of clusters is the precise determination of the
geometrical structure that the constituent atoms adopt. In the
words of Goedecker *et al* [4], 'Determining the structure of a
molecule, cluster, or crystal is one of the most fundamental
and important tasks in solid state physics and chemistry.
Practically all physical properties of a system depend on its
structure.' In view of this, the determination of the actual
geometry a cluster adopts has attracted much interest, and
several strategies to find these minimum energy structures have
been put forward [5–10].

There are basically two approaches to search for minimal
energy cluster structures. The first one is to calculate, via
DFT with or without relaxation, a given set of configurations,
and find the one with the lowest energy. The configurations
are usually chosen to have high symmetry [11, 12], but this
procedure has the drawback that there is no guarantee that
the actual quantum minimum has the chosen symmetry, nor
that the chosen seed, if relaxed via DFT, converges towards

the minimum energy configuration. The second approach is to search for minima in an unbiased fashion (that is, without symmetry restrictions) with a phenomenological potential using global minimizers [13, 14]. In this case, the implicit assumption is that the minimum of the phenomenological potential corresponds to the quantum one (transferability), an assumption which may or may not be valid. A way to improve on the results obtained with this second approach is to perform a DFT refinement of the 'phenomenological' minimum. This should provide a better solution, within the context of the aforementioned transferability assumption. In this paper we improve on this approach, by carrying out a genetic algorithm (GA) search with five different phenomenological potentials followed by DFT refinement. This way we combine the advantages of both approaches: (i) we investigate an initially diverse set of cluster configurations, and (ii) such configurations are the results of an unbiased search. As an additional benefit, we are able to explore which of the phenomenological potentials provides the best seeds for DFT refinement.

Unfortunately, there is not much experimental data on free-standing clusters to compare theoretical results with, or to establish the accuracy of numerically obtained properties and characteristics of putative minima. Recently we studied Pd clusters of up to $N = 13$ atoms using a genetic algorithm with a number of phenomenological potentials to obtain a first approximation of the minimum energy cluster structure. These minimal energy configurations were then refined with DFT approaches, in the search for the minimum energy cluster configuration [14]. For these clusters ($N \leqslant 13$) we found that, independently of the specific phenomenological potential used, the DFT refinement led to the same cluster symmetry as the one obtained using phenomenological potentials. As we will see below, this is not the case for the $N > 14$ structures. Moreover, we will also see that many of the $N > 14$ structures we obtain have very low symmetries that would have been difficult to obtain starting from configurations of high symmetry. This is one of the main results of this paper.

Actually, in a previous paper [13] we found that for $Pd_{13}$ the symmetry preservation paradigm seems to work fine, but at the same time we concluded that this symmetry preservation fails to hold for $Rh_{13}$ and $Ag_{13}$. In fact, a search based on the conformational space annealing method [13] led to different minimal structures when investigating 13-atom rhodium and silver clusters, but for Pd we found that both procedures (phenomenological and *ab initio*) yield a minimum with the same symmetry. We conjecture that this agreement may be due to the closed shell ($[Kr]4d^{10}$) electronic structure of Pd. Moreover, Pd is a fascinating element since it is on the verge of being magnetic in the bulk, which strongly suggests the possibility of interesting features of the magnetic structure of Pd nanoclusters. However, the choice of Pd implies that the results we supply here do not necessarily apply to neighboring elements like Ag or Rh.

The present contribution has several objectives:

(i) to calculate, as a function of cluster size, physical properties of Pd clusters such as symmetries, energies, and interatomic distances, by means of several different phenomenological potentials and with due attention to the large-$N$ limit;

(ii) to complement our previous work [14] by providing the details of the calculation procedures that were employed;

(iii) to extend our previous results [14] to clusters of up to 21 atoms in size, and show that the symmetry of the minimal energy structure for $N > 14$ can be different for the several phenomenological potentials we use;

(iv) to carry out DFT refinement of these seeds in order to obtain a geometric and magnetic configuration [3] of a cluster at zero temperature with as low an energy as feasible; and

(v) to try to establish which phenomenological potential provides the best seeds for DFT refinement.

To do so we use a global minimization method, the genetic algorithm (GA), in conjunction with a variety of phenomenological potentials, to search for a first approximation set of minimum energy configurations. The latter are then refined using the SIESTA [15–17], VASP [18–20] and WIEN2k [21] codes.

Phenomenological potentials have been used extensively since they were first introduced. Possibly the first successful attempt in this context is due to Daw, Foiles and Baskes [22, 23], who put forward a formalism known as the embedded atom method (EAM). This formalism was improved upon by Voter and Chen [24]. Other formalisms, different from EAM but related to it, were put forward by Ducastelle [25], Gupta [26, 27], Sutton and Chen [28] and, more recently, by Murrell and Mottram [29, 30]. All of them are many-body potentials, which were developed by fitting several experimentally obtained values, like the cohesive energy, lattice parameters, and independent elastic constants of the bulk 0 K crystal structure. However, as we will see below, the symmetries of the minimal energy structures derived from phenomenological potentials are often different from the ones obtained using *ab initio* codes. This raises the question as to what extent it is appropriate to use bulk potentials to compute cluster properties, a problem that should be investigated in detail. However, we trust that the shortcomings due to this approximation are at least partially mitigated by the quantum refinement.

In combination with the above phenomenological potentials we implement a GA technique to search for global energy minima [31–33]. The main advantage of the GA over other methods is that the latter show a strong tendency to get stuck in local minima, a problem that the GA manages to alleviate. This feature is also related to the ability of the GA to find minimum energy configurations with low symmetry, an important result of this paper, as already mentioned above.

This paper is organized as follows: after this introduction we present the numerical procedure that we implemented, with details about the GA, the phenomenological potentials and the DFT calculations we performed; in section 3 we present the results, that are analyzed and discussed in section 4, which closes this paper.

## 2. Numerical procedure

The procedure we implement here is to close in on the minimal energy structure using phenomenological potentials and geometrical optimization via a genetic algorithm (GA), which is followed by DFT refinement. The synergy between *ab initio* and classical methods thus allows us to significantly reduce the resources that are required and to expand the set of problems amenable to treatment. In addition, the increased computational speed allows to implement evaluation intensive minimization procedures like the GA, which is discussed in detail below. Alternative minimization methods are abundant in the literature [34, 33, 35, 36]. For example, Sebetci and Güvenç [37] in their study of Pt, have concluded that, for clusters between 22 and 56 atoms, basin hopping Monte Carlo is more efficient than molecular dynamics and thermal quenching, but that with a few exceptions the minimal structures that result are quite similar.

### 2.1. Genetic algorithm

In order to search for the minimum energy cluster structure we use a genetic algorithm (GA), which is a global search technique based on the principles of natural evolution [31, 32]. It has been successfully applied to cluster, nanoparticle and protein structures [34, 33, 35, 36]. In particular, we implement a steady-state GA that uses the coordinates of each atom as our genome, and applies an additional local minimizer (in our case a combination of Simplex and Monte Carlo) within the basin [38]. This combination considerably improves the convergence speed, and has proven to be quite reliable [38, 39]. As is standard in the steady-state GA we choose the parents by the roulette wheel selection method, and specify the fraction of population that is preserved across successive generations (elitism). To originate a new generation we adopt the genetic operators described by Niesse and Mayne [38]. The objective function is, of course, the energy, and the fitness score is obtained by dynamic linear scaling of the raw objective score in each generation.

For a fixed number $N$ of atoms in the cluster, and for each one of the phenomenological potentials, we performed computations for 10 different populations (each of them of 30 individuals). The initial atomic positions were chosen at random under the constraint that the average pair separation should be between 0.7 and 1.3 of the bulk nearest neighbor distance. The elitism percentage we adopt is 30%. This procedure is repeated 5000 times to obtain the 'champion', that is the cluster structure with the lowest energy value for each potential. For small clusters ($N < 14$) these 5000 iterations are sufficient to ensure convergence to the same geometry. However, for clusters with $14 \leqslant N \leqslant 21$ we performed 5000 additional iterations for each one of the phenomenological potentials. We started these additional iterations with 10 different populations (each of them of 30 individuals). In each one of these populations we included the 5 champions found in the 5000 initial iterations (one for each potential used) plus 25 chosen at random. We call this procedure 'hybridization' here.

### 2.2. Many-body potentials

We now outline several details related to the various phenomenological potentials we used in our calculations. Actually, one could think that more elementary pair potentials could be sufficient to achieve the task. However, metals are not properly described by pair potentials. In fact, the dynamic properties and the so-called Cauchy discrepancy of the elastic constants, namely the experimental evidence that for most cubic crystals $c_{11} \neq c_{44}$, are not adequately obtained. Another serious drawback of the use of pair potentials is represented by incorrect estimates of the vacancy formation energies, whose values result in being very nearly equal to the cohesive energies, whereas experimental results indicate that they range around 1/3 of the cohesive energy [27].

As already mentioned, the many-body embedded atom method (EAM) was put forward as an alternative to the use of pair potential models. The EAM assumes that each atom in a solid can be regarded as an impurity embedded in a host which comprises all the rest of the atoms, so that the total electron density is approximated by the superposition of electron densities of individual atoms. Thus, the electron density in the vicinity of each atom can be written as the sum of the density of each atom plus the electron density from all the surrounding ones. By making the simplifying assumption that this background electron density is a constant, an embedding energy is defined as a function of the background electron density of the particular atomic species. These ideas were developed by Daw and Baskes [22], who derived an approximation for the total energy. The values we adopted for the parameters that enter the equations are $Z_0 = 10$, $\alpha = 1.2950$, $\beta = 0.0595$, taken from Foiles *et al* [23]. To apply this method the embedding function, pair repulsions, and atomic densities must be known. Approximate values of the embedding functions and pair interactions can be calculated from the formal definitions of these quantities within the DFT framework.

A different parameterization of the EAM was proposed by Voter and Chen [24], which differs from that of Foiles *et al* [23] primarily in the use of a core–core pair interaction. The values of the parameters we used for Pd were given by Voter and Chen [24], and are $\alpha_M = 1.6629$ Å$^{-1}$, $D_M = 1.4272$ eV, $R_M = 2.3908$ eV and $\beta = 3.4456$ Å$^{-1}$.

The Sutton–Chen [28] potential is based on the empirical many-body potential developed by Finnis–Sinclair [40] to describe the cohesion of metals. For these potentials the total internal energy is represented by a cohesive functional of pairwise interactions and a predominantly repulsive pair potential. The main difference of this potential from ordinary pair potentials is that when calculating the force exerted by one atom on another using pair potentials it depends exclusively on the interatomic distance, whereas in the Sutton–Chen scheme it depends on all the neighbors of both atoms. For Pd the parameters we used are $n = 12$, $m = 7$, $a = 3.89$ Å$^{-1}$, $\epsilon = 4.179 \times 10^{-3}$ eV and $c = 108.526$, as given by Rafii-Tabar and Sutton [41]. These values yield a bond length of 2.388 Å, lower than the experimental dimer bond length [42] of 2.48 Å.

The Gupta potential [27] was derived from Gupta's expression for the cohesive energy of the bulk material [26] and is based on the second moment approximation to tight binding theory. It has a very simple analytical form which depends on five parameters. It is written in terms of a repulsive pair potential and an attractive many-body term. The values we adopted for the Pd parameters were taken from Cleri and Rosato [27]; for Pd they are $A = 0.1746$ eV, $\xi = 1.718$ eV, $p = 10.867$, $q = 3.742$ and $r_0 = 2.75$ Å.

An alternative approach was put forward by Murrell and Mottram, who write the potential [29] as a sum of two- and three-body terms. The values we adopted for the parameters are the ones given by Cox *et al* [30], which are $a_2 = 7.0$, $a_3 = 10.2$, $D = 0.946$ eV, $r_e = 2.667$ Å, $c_0 = 0.197$, $c_1 = -0.221$, $c_2 = 6.516$, $c_3 = -0.435$, $c_4 = 10.273$, $c_5 = -14.543$ and $c_6 = 4.463$.

We use the minimal energy configurations obtained with the five phenomenological potentials as seeds and refine them with first-principles calculations using the SIESTA, VASP and WIEN2k codes with geometrical relaxation. Following Alexandre *et al* [43, 44], in all DFT calculations we limited ourselves to the local spin density approximation (LSDA) since it yields good results for Pd. In fact, these authors showed that the generalized gradient approximation (GGA) is not necessarily more reliable for studying Pd, and in particular its magnetism. On the other hand, the LSDA yields a bulk lattice constant in agreement with experiment.

### 2.3. DFT SIESTA code implementation

The SIESTA (Spanish initiative for electronic simulations with thousands of atoms) calculations were performed within the framework of DFT [45, 46], using a basis set of strictly localized numerical pseudoatomic orbitals, as implemented in the SIESTA code [15–17]. The exchange–correlation energy was calculated within the local spin density approximation (LSDA) as parameterized by Perdew and Wang [47]. Norm-conserving pseudopotentials[3] [48], in their non-local form, were used to describe the electron–ion interaction, including non-linear core corrections [49]. We have used a double-zeta basis set including polarization functions (DZP) [16, 50]. The clusters were placed in a cubic supercell of up to 20 Å per side. Due to the large size of the supercell only the Γ point was evaluated to sample the Brillouin zone. The cluster geometries obtained by means of the GA were fully relaxed using the conjugate gradient method, without any symmetry constraint, until all the force components became smaller than 0.01 eV Å$^{-1}$. The geometry of each cluster was minimized, allowing the spin multiplicity to vary freely.

### 2.4. DFT VASP code implementation

We also used the *ab initio* VASP (Vienna *Ab Initio* Simulation Program) code [18–20] with a plane-wave basis and PAW ultrasoft [51, 52] pseudopotentials. The kinetic energy cutoffs used were the maximal default values recommended by the pseudopotential database, namely 250 eV. For the exchange–correlation functional we used the spin polarized local density

[3] Available at http://www.uam.es/departamentos/ciencias/fismateriac/siesta/.

approximation [47]. A cubic supercell with a side dimension of 20 Å was employed in the calculation. Only the Γ point was evaluated in the Brillouin zone integration, since $3 \times 3 \times 3$ Monkhorst–Pack *k*-point mesh computations, where all the atoms are allowed to relax following Hellmann–Feynman forces, yield equivalent results for the total energy. The cluster geometry is optimized, without symmetry constraints, until the total energy is converged to $10^{-4}$ eV in the self-consistency loop and the force on each atom is less than 0.05 eV Å$^{-1}$. The energy spread $\sigma$ was set equal to 0.02 eV.

### 2.5. DFT WIEN code implementation

In order to check the reliability of our calculations we performed all-electron DFT calculations of the total energies for the smaller clusters, using the full-potential linearized augmented plane-wave method (FP-LAPW) [21]. The WIEN2k code is an implementation of DFT which allows different approximations for the exchange and correlation potential, including the local spin density approximation (LSDA). For the exchange and correlation potential we used the Perdew and Wang parameterization of the Ceperley–Alder approximation of the local density approximation [47]. The Kohn–Sham equations are solved using a basis of linearized augmented plane waves [53]. Local orbital extensions to the LAPW basis were used to describe the 4s and 4p orbitals of Pd.

The wavefunctions are expanded up to $\ell_{max} = 10$ within the muffin-tin spheres, and the potential and charge densities are expanded up to $G_{max} = 10$. For Pd we use a converged basis set of around 7000 plane waves and a muffin-tin radius of 2.2 bohr. The cell is cubic with a side of 15 Å and only the Γ point is considered for Brillouin zone integrations.

## 3. Results and discussion

### 3.1. DFT configurations and symmetries

As already mentioned, the GA we use consists of a combination of local minimizers, genetic operations and 'hybridization' to search for a global minimum, and was outlined in section 2.1. The phenomenological minima thus obtained were subsequently refined by means of DFT calculations. The geometries adopted by the putative minimum energy Pd clusters ($14 \leqslant N \leqslant 21$) are displayed in figure 1, and the symmetries that determine the point groups are given in table 1. On the left-hand side of figure 1 we show the minimum energy configurations we obtained using several phenomenological potentials. On the right of the vertical line in figure 1 are the refined configurations obtained with SIESTA and VASP. Table 1 summarizes the average nearest neighbor distances (specified below), and the space group of the corresponding configuration, obtained with the phenomenological potentials and with the SIESTA and VASP codes. In a few cases we were unable to assign a symmetry group to the cluster.

In relation to the structure symmetries displayed in figure 1 we notice that, contrary to our own findings [14] for clusters of up to 13 atoms, several DFT symmetries
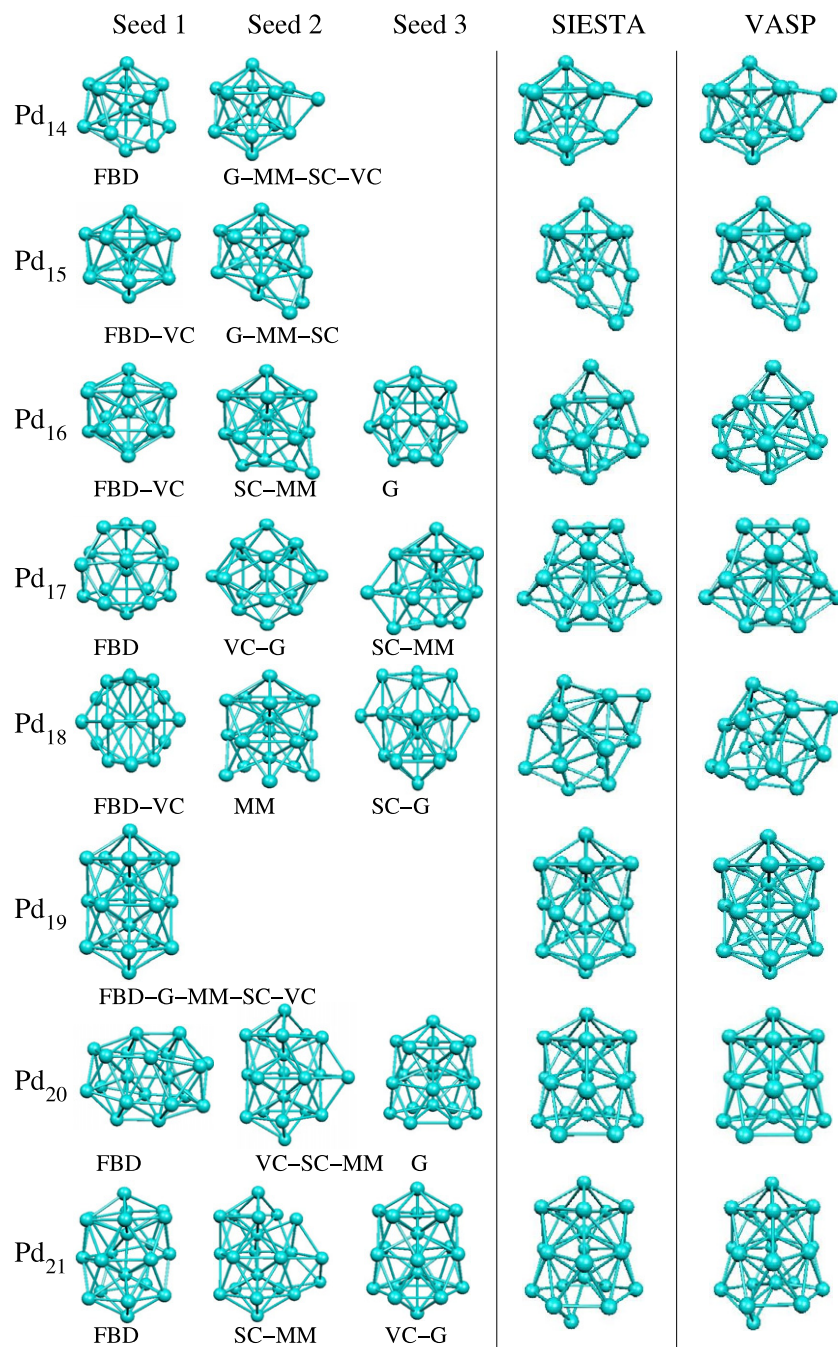
**Figure 1.** Illustration of the structures that the different size clusters adopt. On the left of the vertical line are the results obtained using phenomenological potentials in combination with the genetic algorithm. On the right are results obtained with the SIESTA and VASP codes after relaxation of the phenomenological results. FBD: Foiles–Baskes–Daw, G: Gupta, MM: Murrell–Mottram, SC: Sutton–Chen, VC: Voter–Chen.

obtained for the refined structures differ from those obtained phenomenologically. This fact is especially conspicuous for $N = 16$, 17 and 18, but is also present for $N = 20$ and 21. We observe that all phenomenological potentials, except FBD and VC, yield the minimal structure for $N = 14$ and 15, respectively. In fact the latter differ only slightly from the DFT results. The $N = 19$ cluster constitutes a special case; while all but one of the phenomenological potentials and VASP yield the same symmetry group ($C_5$), SIESTA yields a structure that looks quite similar, and has the same average

nearest neighbor (nn) distance as MM; however, its symmetry is $D_{5h}$.

We now turn our attention to the comparison of the nn distance of the different clusters. For the minimum energy configurations obtained with the SIESTA and VASP codes (see figure 1), we computed all the possible distances between atoms of a given cluster to construct the pair distance distribution. In figure 2 we show the number of atomic pairs $p(r)$ with a bond length within a bin of width $\delta x = 0.05$ Å. From this plot we can conclude that a reasonable definition for

**Table 1.** Point symmetry group and average nearest neighbor interatomic distance *d* for the Pd clusters illustrated in figure 1. FBD: Foiles–Baskes–Daw, G: Gupta, MM: Murrell–Mottram, SC: Sutton–Chen, VC: Voter–Chen, and SG: symmetry group.

| | FBD | | VC | | G | | SC | | MM | | SIESTA | | VASP | |
|---|---|---|---|---|---|---|---|---|---|---|---|---|---|---|
| | $d$ (Å) | SG | $d$ (Å) | SG | $d$ (Å) | SG | $d$ (Å) | SG | $d$ (Å) | SG | $d$ (Å) | SG | $d$ (Å) | SG |
| 14 | 2.62 | $C_{2v}$ | 2.63 | $C_{3v}$ | 2.65 | $C_{3v}$ | 2.68 | $C_{3v}$ | 2.72 | $C_{3v}$ | 2.72 | $C_{3v}$ | 2.66 | $C_{3v}$ |
| 15 | 2.63 | $C_6$ | 2.66 | $C_6$ | 2.65 | $C_{2v}$ | 2.67 | $C_{2v}$ | 2.72 | $C_{2v}$ | 2.71 | $C_{2v}$ | 2.65 | $C_2$ |
| 16 | 2.64 | $D_{3h}$ | 2.66 | $D_{3h}$ | 2.65 | $C_s$ | 2.67 | $C_s$ | 2.73 | $C_s$ | 2.68 | $C_s$ | 2.65 | $C_s$ |
| 17 | 2.64 | $T_d$ | 2.63 | $C_{2v}$ | 2.66 | $C_{2v}$ | 2.67 | $C_2$ | 2.71 | $C_2$ | 2.70 | $C_{2v}$ | 2.65 | $C_{2v}$ |
| 18 | 2.62 | $C_{2v}$ | 2.65 | $C_{2v}$ | 2.65 | | 2.66 | $C_5$ | 2.73 | $C_s$ | 2.68 | | 2.64 | |
| 19 | 2.65 | $C_5$ | 2.66 | $C_5$ | 2.67 | $C_5$ | 2.70 | $D_{5h}$ | 2.73 | $C_5$ | 2.73 | $D_{5h}$ | 2.68 | $C_5$ |
| 20 | 2.63 | $D_{3d}$ | 2.65 | $C_{2v}$ | 2.65 | $C_s$ | 2.70 | $C_{2v}$ | 2.73 | $C_{2v}$ | 2.70 | | 2.64 | $C_s$ |
| 21 | 2.65 | $C_s$ | 2.66 | | 2.66 | | 2.68 | | 2.73 | | 2.71 | | 2.64 | |
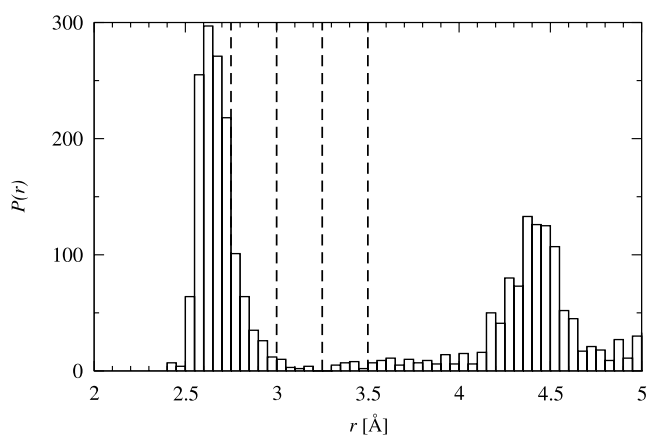


**Figure 2.** Number of atomic pairs $P(r)$, computed for the minimum energy configurations obtained with the SIESTA and VASP codes. As references we display the distances $r = 2.75$, 3.0, 3.25 and 3.5 Å as vertical lines.



**Figure 3.** Average nearest neighbor distance for the various potentials and for DFT (SIESTA and VASP). The horizontal line corresponds to the bulk value. FBD: Foiles–Baskes–Daw, G: Gupta, MM: Murrell–Mottram, SC: Sutton–Chen, VC: Voter–Chen.

the size of the first shell is $r_c \approx 3.0$ Å, which we use from now on to define the cutoff distance for the nearest neighbors of an atom; moreover, this is consistent with the literature [14]. In figure 3 the average nn distance is plotted as a function of cluster size, for the different potentials that we investigated. Starting from the dimer [54, 55], the bond length increases with growing cluster size to a value quite close to 2.74 Å, the experimental bulk nn distance [56]. For bulk Pd (fcc), SIESTA yields a bond length of 2.763 Å and VASP yields 2.795 Å.

It is also of interest to mention that we computed the number of atoms in our Pd clusters with coordination equal to 12 (the bulk value), in order to the develop a feeling on how soon a cluster attains bulk characteristics. It turns out that the number of atoms with bulk coordination is zero for $N < 13$, 1 for $N = 13$ and 2 for $N = 19$. To reach a fraction of 90% of the cluster atoms with bulk coordination we estimate that the cluster has to contain no fewer than $N \approx 20\,000$ atoms.

### 3.2. First and second differences

As mentioned above, we feed the minimal energy structures obtained via phenomenological potentials into the DFT codes. It is of interest to observe which input data eventually lead to what results. This information is displayed in figure 4, where
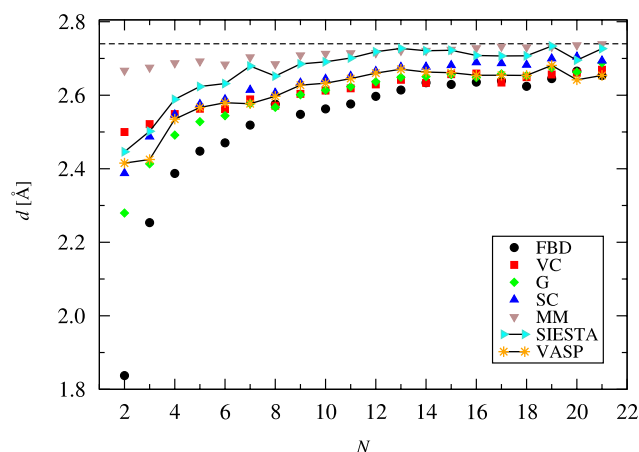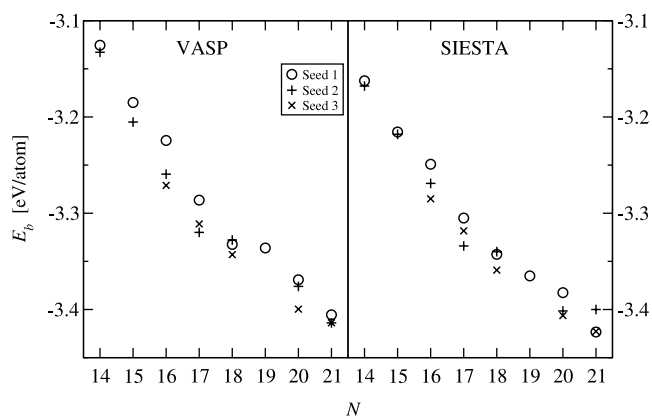


**Figure 4.** Binding energies for the various isomers, after refining with VASP and SIESTA the structure of the seeds obtained with the various phenomenological potentials, and displayed and labeled in figure 1.

the binding energies $E_b$ computed using SIESTA and VASP, starting from the different seeds illustrated in figure 1, are displayed. The consistency of the results is quite satisfactory and constitutes an indication of the reliability and accuracy of the computation methods we employed. In addition, a
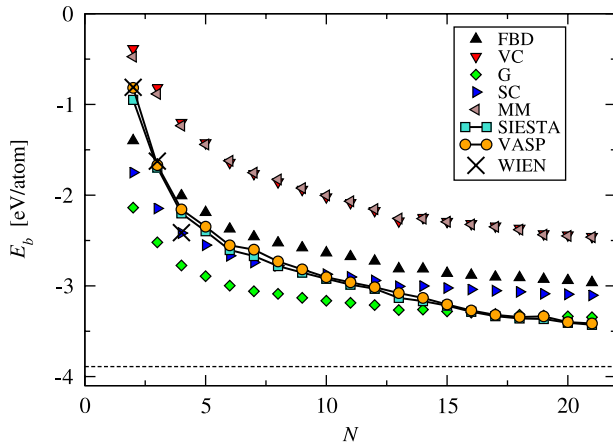
**Figure 5.** Energy per atom as a function of cluster size for the various potentials and for DFT (SIESTA, VASP and WIEN). The horizontal line corresponds to the bulk value. FBD: Foiles–Baskes–Daw, G: Gupta, MM: Murrell–Mottram, SC: Sutton–Chen, VC: Voter–Chen. The lines connecting the DFT SIESTA and VASP results are a guide to the eye.



**Figure 6.** First difference for the various potentials and for DFT (SIESTA and VASP). FBD: Foiles–Baskes–Daw, G: Gupta, MM: Murrell–Mottram, SC: Sutton–Chen, VC: Voter–Chen.



**Figure 7.** Second difference for the various potentials and for DFT (SIESTA and VASP). FBD: Foiles–Baskes–Daw, G: Gupta, MM: Murrell–Mottram, SC: Sutton–Chen, VC: Voter–Chen.

general trend that appears is the good performance of the Gupta potential as source of candidates (seeds) for DFT refinement.

In order to investigate the relative stabilities of the clusters we consider the evolution of the binding energy $E_b$, the first and second energy differences $\Delta_1 E$ and $\Delta_2 E$, respectively, all defined in terms of the total interaction energy of the cluster $V_{\text{cluster}}$. Analytically

$$E_b(N) = \frac{V_{\text{cluster}}}{N} \qquad (1)$$

$$\Delta_1 E = E_b(N) - E_b(N-1) \qquad (2)$$

$$\Delta_2 E = 2E_b(N) - E_b(N-1) - E_b(N+1). \qquad (3)$$

Our results for $E_b$ as a function of $N$ are displayed in figure 5. As expected, in the very large cluster limit $E_b$ approaches the cohesive energy of the corresponding bulk solid (for Pd $E_b = -3.89$ eV/atom), as the difference in binding energy of clusters and bulk becomes smaller and smaller.

The magnitude of $\Delta_1 E$ is a measure of the relative stability of a cluster against the loss of one of its constituent atoms ($\Delta_1 E = 0$ for the bulk). An important feature of the $\Delta_1 E$ graph displayed in figure 6 is the relative minimum at $N = 13$, which corresponds to a region of enhanced stability (magic number).

On the other hand, a minimum of $\Delta_2 E$ indicates an enhanced stability of a cluster, relative to its heavier and lighter neighbors. Therefore, $\Delta_2 E$ can be considered a measure of the stability of the clusters, which in general is correlated with experimental mass spectral intensities rather than with the binding energy $E_b$. Thus, the minima of $\Delta_2 E$ identify the clusters which are most stable. In particular, the deep minimum of $\Delta_2 E$ we observe for $N = 13$ in figure 7, for all phenomenological potentials and DFT calculations, indicates an enhanced stability of the 13-atom cluster (magic number). Except for $N = 19$, the agreement between results obtained for $\Delta_2 E$ using phenomenological potentials and DFT calculations is quite reasonable.
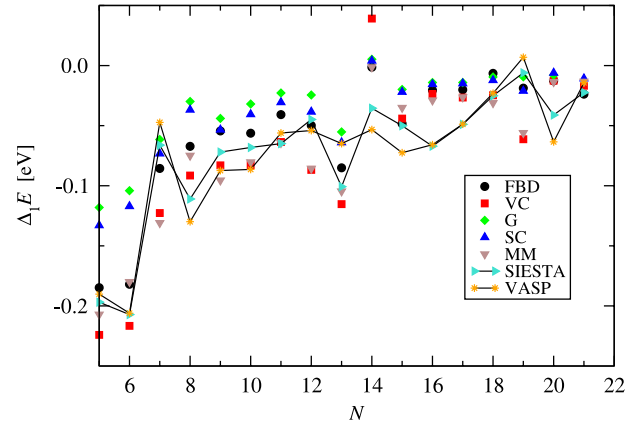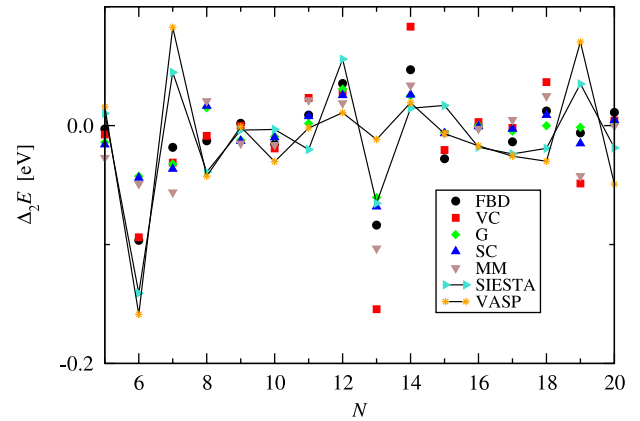
It is interesting to notice that, as $N$ grows, an improving agreement for the binding energies and bond lengths is observed when comparing phenomenological and DFT results. Moreover, the small differences between the results obtained using the Voter–Chen, Sutton–Chen and Gupta potentials as compared with the DFT results, over the whole range $2 \leqslant N \leqslant 21$, is quite remarkable. The variation between the SIESTA and VASP values, with the latter being always smaller, is probably due to the way nearest and second nearest neighbors are defined, and to small differences in the cutoff radii of the respective pseudopotentials.

### 3.3. Magnetic moments

In figure 8 we display the magnitude of the total magnetic moment $\mu$, in units of Bohr magnetons, of the lowest energy configuration of the various clusters described above. Our values for $\mu$ differ from recent results found in the literature [57, 58], but obtained for slightly different structures from ours. In fact, Kumar and Kawazoe [57] report for $N = 7$ four different structures, that differ in energy by a few meV, and for which $\mu = 0$, 2 and 4. Futschek *et al* [58] also report
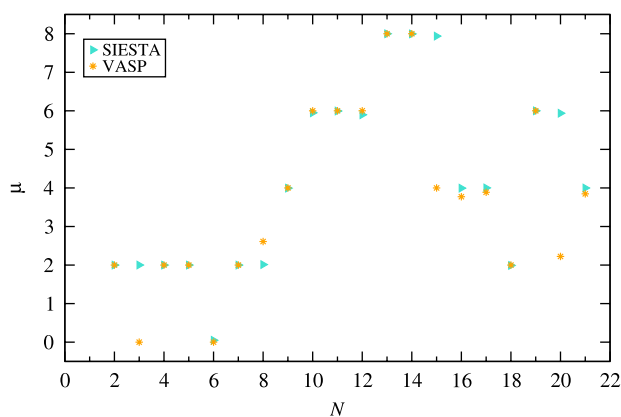
**Figure 8.** Magnetic moment per atom versus cluster size of the lowest energy configuration, after relaxation with SIESTA and VASP.

several 7-atom Pd $\mu = 0$ and 2 structures, whose energies differ by a few meV. The total energy difference between the $N = 7$ cluster with $\mu = 0$ and 1 that we obtain is 62 meV. For the $N = 10$ cluster the difference between the $\mu = 1$ and 2 configurations amounts to 158 meV.

However, for $N = 3, 8, 15$ and 20 the values of the magnetic moments obtained by SIESTA and VASP are significantly different. We thus checked the magnitude of the magnetic moment $\mu$, for the above values of $N$, by recalculating them using SIESTA with fixed spin values, at the magnitude given by VASP. The results are the following: (i) for $N = 3$ and 8 the value $\mu = 2$ continues to have the lowest energy; (ii) for $N = 15$ SIESTA yields $\mu = 8$ and VASP $\mu = 4$. We calculated for several values between $\mu = 4$ and 8 and found that $\mu = 6$ is lower in energy than the other two, but by only $\approx 0.1$ eV; and (iii) for $N = 20$ the energies of the $\mu = 6$ given by SIESTA and $\mu = 2.2$ given by VASP differ by less than $10^{-4}$ eV. We conclude that, in general, due to the large difference in magnitude between elastic and magnetic energies, the latter are extremely sensitive to minute geometry changes. This implies that the exact determination of the minimum energy configuration becomes very difficult, suggesting that at finite temperatures several magnetic cluster configurations will quite often coexist.

## 4. Summary and conclusions

We have calculated, via several phenomenological potentials in combination with the GA followed by DFT refinement, the geometrical structure, total energy and magnetic configuration of Pd$_{14}$ through Pd$_{21}$ clusters. This constitutes an extension of a recently published work for Pd clusters of $2 \leqslant N \leqslant 13$ atoms [14]. Since Pd has a closed shell atomic configuration our results do not necessarily apply to neighboring elements, like Ag or Rh.

Many minimization techniques are presently in use, like basin hopping Monte Carlo, thermal quenching, molecular dynamics, simulated annealing, genetic algorithm and conformational space annealing. They differ in efficiency and the computer resources and time required to implement them.

We have chosen the genetic algorithm in combination with Simplex and Monte Carlo methods, as local minimizers, to zero in on the local minima. The procedure proves to be quite efficient and mitigates the pitfall of getting stuck in local minima.

In this context phenomenological potentials are quite successful in closing in on the minimal energy geometrical structure of Pd clusters smaller than 16 atoms. Unfortunately, they start failing from that size onwards as far as the symmetry group of the structure is concerned. However, the general trends for interatomic distances, binding energies and first and second differences are very satisfactory, even for the largest cluster sizes we report here (see figures 3 and 5–7). Furthermore, phenomenological potentials seem to provide a convenient input for SIESTA, VASP and other DFT implementations, thus allowing us in the case of Pd to save computer time. The question that remains open is how adequate phenomenological potentials, developed on the basis of bulk properties, are in describing clusters. However, we trust to be able to shed some light on this issue shortly. Nevertheless, in this context the accuracy of the easily implemented Gupta potential [26], in the range $14 \leqslant N \leqslant 21$, is quite remarkable.

A general conclusion we draw is that high symmetry does not guarantee success when used as a starting point criterion in the search of the minimum energy configurations. This is particularly relevant when biased searches are performed, by discarding *a priori* lower symmetry geometries and allowing relaxation of just the higher symmetry configurations, since the latter may be separated from the low symmetry absolute minimum by an unsurmountable energy barrier. To handle these difficulties we have developed a search scheme focused on preserving diversity [13], whose full details will be published elsewhere shortly.

As far as the magnetic configurations are concerned, we observe a trend to larger magnetic moments with increasing cluster size, but this trend is far from smooth and is associated to some degree of uncertainty. In fact, the large difference between the elastic and magnetic energy scales implies that slight uncertainties in the interatomic distances bring about qualitatively different results for the magnetic configurations [57, 58].

## References

[1] Bansmann J *et al* 2005 *Surf. Sci. Rep.* **56** 189 and references therein
[2] Held A, Kolb L, Zuideveld M A, Thomann R, Mecking S, Schmid M, Pietruschka R, Lindner E, Sunjuk M and Khanfar M 2002 *Macromolecules* **35** 3342

[3] Shinohara T, Sato T and Taniyama T 2003 *Phys. Rev. Lett.* **91** 197201

[4] Goedecker S, Hellmann W and Lenosky T 2005 *Phys. Rev. Lett.* **95** 055501

[5] Juhás P, Duxbury P M, Punch W F and Billinge S L 2006 *Nature* **440** 655 and references therein

[6] Joswig J O and Springborg M 2003 *Phys. Rev. B* **68** 085408

[7] Grigoryan V G and Springborg M 2003 *Chem. Phys. Lett.* **375** 219

[8] Grigoryan V G and Springborg M 2004 *Phys. Rev. B* **70** 205415

[9] Grigoryan V G, Alamova D and Springborg M 2006 *Phys. Rev. B* **73** 115415

[10] Dong Y and Springborg M 2007 *J. Phys. Chem.* C **111** 12528

[11] Chang C M and Chou M Y 2004 *Phys. Rev. Lett.* **93** 133401

[12] Li X, Li J, Zhai H-J and Wang L-S 2003 *Science* **299** 864

[13] Rogan J, García G, Loyola C, Orellana W, Ramírez R and Kiwi M 2006 *J. Chem. Phys.* **125** 214708

[14] Rogan J, García G, Valdivia J A, Orellana W, Romero A H, Ramírez R and Kiwi M 2005 *Phys. Rev. B* **72** 115421

[15] Ordejón P, Artacho E and Soler J M 1996 *Phys. Rev. B* **53** R10441

[16] Soler J M, Artacho E, Gale J D, García A, Junquera J, Ordejón P and Sánchez-Portal D 2002 *J. Phys.: Condens. Matter* **14** 2745

[17] Soler J M, Beltran M R, Michaelian K, Garzón I L, Ordejón P, Sánchez-Portal D and Artacho E 2000 *Phys. Rev. B* **61** 5771

[18] Kresse G and Hafner J 1993 *Phys. Rev. B* **47** 558

[19] Kresse G and Furthmüller J 1996 *Comput. Mater. Sci.* **6** 15

[20] Kresse G and Furthmüller J 1996 *Phys. Rev. B* **54** 11169

[21] Blaha P, Schwarz K, Madsen G K H, Kvasnicka D and Luitz J 2001 *WIEN2k, An Augmented Plane Wave + Local Orbitals Program for Calculating Crystal Properties* Karlheinz Schwarz, Techn. Universität, Wien, Austria

[22] Daw M S and Baskes M I 1984 *Phys. Rev. B* **29** 6443

[23] Foiles S M, Baskes M I and Daw M S 1986 *Phys. Rev. B* **33** 7983

[24] Voter A F and Chen S P 1987 *Characterization of Defects in Materials* (*MRS Symp. Proc.* vol 82) ed R W Siegal, J R Weertman and R Sinclair (Warrendale, PA: Materials Research Society) p 175

[25] Ducastelle F 1970 *J. Physique* **31** 1055

[26] Gupta R P 1985 *Phys. Rev. B* **23** 6265

[27] Cleri F and Rosato V 1993 *Phys. Rev. B* **48** 22

[28] Sutton A P and Chen J 1990 *Phil. Mag. Lett.* **61** 139

[29] Murrell J N and Mottram R E 1990 *Mol. Phys.* **69** 571

[30] Cox H, Johnston R L and Murrell J N 1990 *J. Solid State Chem.* **145** 571

[31] Holland J 1975 *Adaptation in Natural and Artificial Systems* (Ann Arbor, MI: University of Michigan Press)

[32] Goldberg D E 1989 *Genetic Algorithms in Search, Optimizations and Machine Learning* (Reading, MA: Addison-Wesley)

[33] Mitchell M 1998 *An Introduction to Genetic Algorithms* (Cambridge, MA: MIT Press)

[34] Deaven D M, Tit N, Morris J R and Ho K M 1996 *Chem. Phys. Lett.* **256** 195

[35] Michaelian K, Rendón N and Garzón I L 1999 *Phys. Rev. B* **60** 2000

[36] Johnston R L 2003 *J. Chem. Soc. Dalton Trans.* (22) 4193

[37] Sebetci A and Güvenç Z B 2004 *Eur. Phys. J.* D **30** 71

[38] Niesse J A and Mayne H R 1996 *J. Chem. Phys.* **105** 4700

[39] Iwamatsu M 2000 *J. Chem. Phys.* **112** 109760

[40] Finnis M W and Sinclair J E 1984 *Phil. Mag.* A **50** 45

[41] Rafii-Tabar H and Sutton A P 1991 *Phil. Mag. Lett.* **63** 217

[42] Balasubramanian K 1988 *J. Chem. Phys.* **89** 6310

[43] Alexandre S S, Mattesini M, Soler J M and Yndurain F 2006 *Phys. Rev. Lett.* **96** 079701

[44] Alexandre S S, Anglada E, Soler J M and Yndurain F 2006 *Phys. Rev. B* **74** 054405

[45] Hohenberg P and Kohn W 1964 *Phys. Rev. B* **136** 834

[46] Kohn W 1999 *Rev. Mod. Phys.* **71** 1253

[47] Perdew J P and Wang Y 1992 *Phys. Rev. B* **45** 13244

[48] Troullier N and Martins J L 1991 *Phys. Rev. B* **43** 1993

[49] Louie S G, Froyen S and Cohen M L 1982 *Phys. Rev. B* **26** 1738

[50] Junquera J, Paz O, Sánchez-Portal D and Artacho E 2001 *Phys. Rev. B* **64** 235111

[51] Kresse G and Joubert D 1999 *Phys. Rev. B* **59** 1758

[52] Kresse G and Hafner J 1994 *J. Phys.: Condens. Matter* **6** 8245

[53] Singh D 1994 *Plane Waves, Pseudopotentials, and the LAPW Method* (New York: Kluwer–Academic)

[54] Ho J, Ervin K M, Polak M L, Gilles M K and Lineberger W C 1991 *J. Chem. Phys.* **95** 4845

[55] Moseler M, Häkkinen H, Barnett R N and Landman U 2001 *Phys. Rev. Lett.* **86** 2545

[56] Kittel C 1986 *Introduction to Solid State Physics* (New York: Wiley)

[57] Kumar V and Kawazoe Y 2002 *Phys. Rev. B* **66** 144413

[58] Futschek T, Marsman M and Hafner J 2005 *J. Phys.: Condens. Matter* **17** 5927